IEEE/CSC & ESAS EUROPEAN SUPERCONDUCTIVITY NEWS FORUM (ESNF), No. 11, January 2010
Published in *Journal of Physics Conf. Series* (*SuST*) **234**, 022019 (2010)

Modelling of transient state phenomena of composite superconducting conductors during pulse $I_c(B)$ measurements

S. Krosny[1], M. Woźniak[2], S. C. Hopkins[2], M. A. Stępień[1], B. Grzesik[1], B. A. Glowacki[2]

[1]Department of Power Electronics, Electrical Drives and Robotics, Silesian University of Technology, Gliwice, Poland

[2]Department of Materials Science and Metallurgy, University of Cambridge, Cambridge, United Kingdom

Corresponding author: sebastian.krosny@polsl.pl

Abstract. Computational modelling of pulsed current characterisation in composite superconducting conductors has been performed as the first step towards understanding the electromagnetic processes occurring during pulse $I_c(B)$ measurements in the Cryo-BI-Pulse System. A simplified 2D model was created using the Finite Element Method (FEM) software ANSYS to investigate the current transfer process in a multifilamentary conductor, resulting in time dependent 2D distributions of electrical potential and current density along the wire axis. Experimental measurements were performed for two dissimilar NbTi wires and MgB_2 tape: excellent agreement between pulse and DC results were found for one NbTi wire and the MgB_2 tape, but the critical current for the other NbTi wire (Luvata OK3900) was significantly lower in pulsed current than DC characterisation. This behaviour has been interpreted in relation to current transfer phenomena using results from the FEM modelling.

1. Introduction

The use of pulsed magnetic fields and currents for transport critical current characterisation has many potential benefits, but introduces challenges in obtaining measurements consistent with conventional DC characterisation for some types of sample. Current transfer is expected to be a significant factor affecting measurements of short straight samples [1], as used in the pulsed measurements reported here, and two kinds may be identified. The first is the initial transfer of current from the current leads into the conductor filaments: the heat generated on passing through the ohmic matrix and contacts is greatly reduced by using a short pulse of current. The second is the current transfer process distributing the current amongst the filaments. These processes depend on the detailed structure and materials in the composite conductor including the size and distribution of the filaments and the resistivity of the matrix.

To investigate this behaviour two dissimilar NbTi wires (Luvata OK3900 and IMI A60/25) and a MgB_2 tape (Columbus Superconductors) were measured using a pulsed current - pulsed field system and the results compared to DC measurements reported by the manufacturers. In parallel, Finite Element Method (FEM) modelling of the response to a current pulse matching the experimental conditions was performed using a geometry based on OK3900, for two different interfilamentary

matrix materials. Comparison of the experimental and modelling results allowed the influence of matrix resistivity, wire architecture and other factors to be assessed.

2. Methods

2.1. Experimental

The Cryo-BI-Pulse system and technique was previously described in [2-6]. The system delivers magnetic field and current pulses by the discharge of capacitor banks. Magnetic fields up to 26 T and currents up to 700 A can be achieved. During a magnetic field pulse (13.8 ms) (figure 1) created by a resistive coil, a 3.8 ms current pulse is discharged through a sample immersed in liquid helium and placed in the bore of the coil perpendicular to the magnetic field. The voltage recorded from the sample (figure 2) is corrected to eliminate the voltages induced by pulsed fields. The smallest value of the pulse current in magnetic field for which the wire shows a resistive peak of voltage (solid line in the figure 2) is treated as the critical current value.

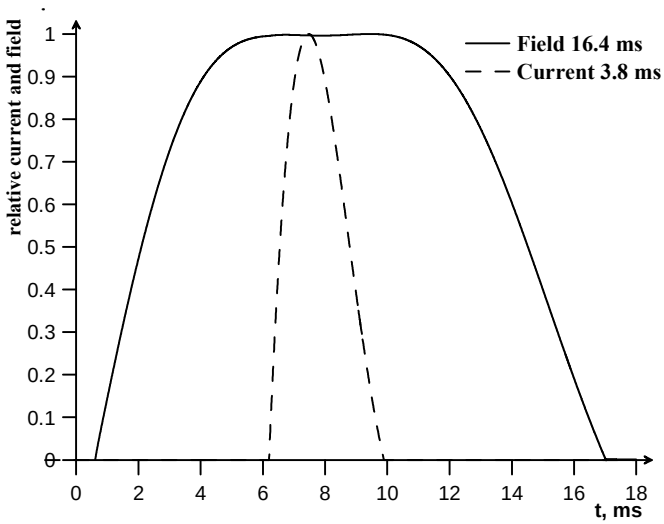

Figure 1. Shape and timing of the magnetic field and current pulses used in the Cryo-BI-Pulse system for critical current measurement.

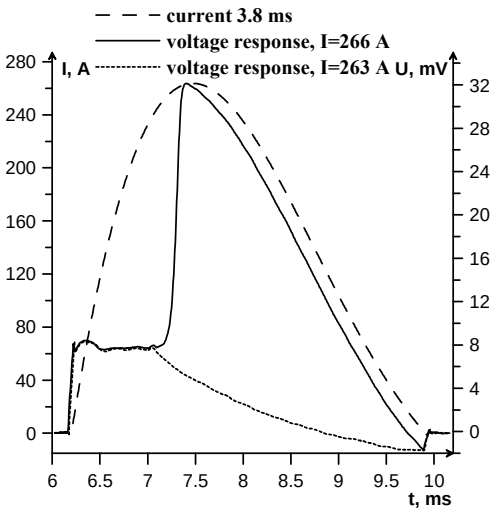

Figure 2. Voltage response for a current below (I=263 A) and above (I=266 A) the critical current I_c during a 4 T magnetic field pulse (not shown).

Two sample geometries were tested: short straight wires and U-shaped hairpins. The short straight samples were 10 mm long and placed perpendicular to the pulsed magnetic field. The hairpin samples were 80 mm long and bent into a U shape, with voltage taps on the section perpendicular to the magnetic field. In both cases, the voltage taps were 5 mm apart, in the middle of the length between the current leads. Cross sections of the investigated conductors are shown in figure 3.

2.2. Modelling

A 2D model (figure 4) with axial and planar symmetry was used in the FEM analysis corresponding to the 3D geometry shown in figure 5. A simplified geometry was used to represent a multifilamentary wire, consisting of two coaxial NbTi cylinders separated from each other, and the internal and external copper, by 1μm layers. Calculations were performed first using CuMn and then Cu for these layers. The volume fractions of NbTi and copper match the NbTi/CuMn/Cu wire (OK3900) investigated experimentally. To allow a transient coupled electromagnetic-circuit analysis, current was injected to the clamp using electrical circuit element CIRCU124 [10].

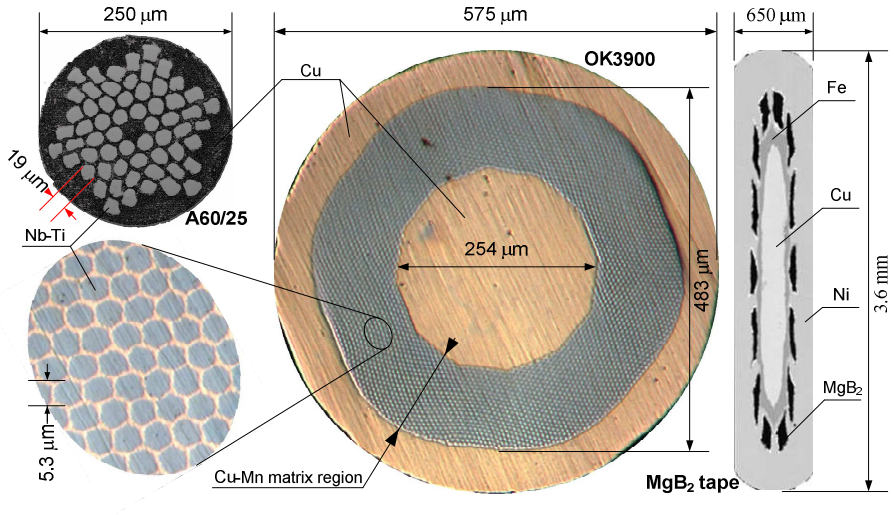

Figure 3. Cross sections of the two NbTi wires and one MgB_2 tape investigated.

The model was designed to investigate current transfer processes without external magnetic field, and for simplicity it does not take into account the magnetic field and temperature dependence of the critical current density. The resistivity of the NbTi material was dynamically and iteratively calculated for each mesh element from the equation: $\rho=\rho_0(J/J_c)^n$ [8]. A half-cycle sinusoidal pulse of current was applied (amplitude 800 A, period 3.8 ms) corresponding to the experimental current pulse. The model parameters were: $\rho_0=10^{-14}$ Ωm, n=50, $J_c=6\cdot10^9$ A/m^2, $r_{Cu} = 2\cdot10^{-10}$ Ωm, $r_{CuMn}= 2\cdot10^{-8}$ Ωm.

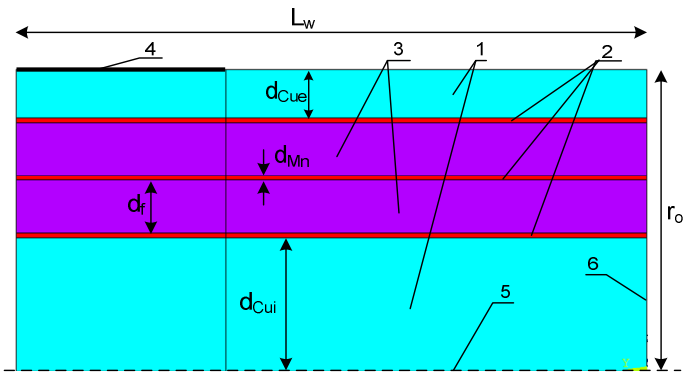

Figure 4. Area of 2D model (not to scale): 1– Cu, 2– Cu or CuMn, 3–NbTi, 4 –clamp, 5 – axis of symmetry, 6–plane of symmetry. Dimensions: L_w – 5 mm, r_o – 287.5 µm, d_{Cui} – 125 µm, d_{mn} – 1 µm, d_{Cue} – 48 µm, d_f – 55.75 µm, clamp – 2 mm.

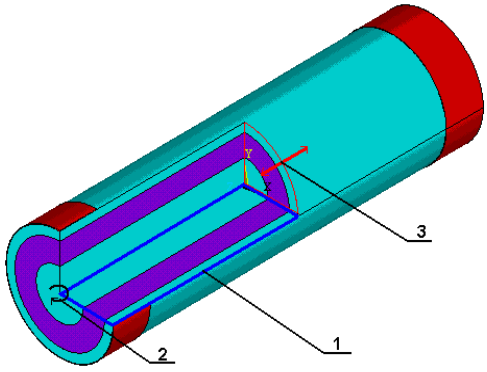

Figure 5. 3D representation of the 2D model geometry: 1 – area of 2D model, 2 – axial symmetry, 3 – planar symmetry.

3. Results and Discussion

3.1. Experimental

The measurements performed on straight samples of the multifilamentary NbTi/Cu (IMI A60/25) wire and MgB_2/Ni/Fe/Cu (Columbus Superconductors) tape using the Cryo-BI-Pulse system gave critical current values in very good agreement with DC measurements obtained by the manufacturers [4,5] (figure 6).

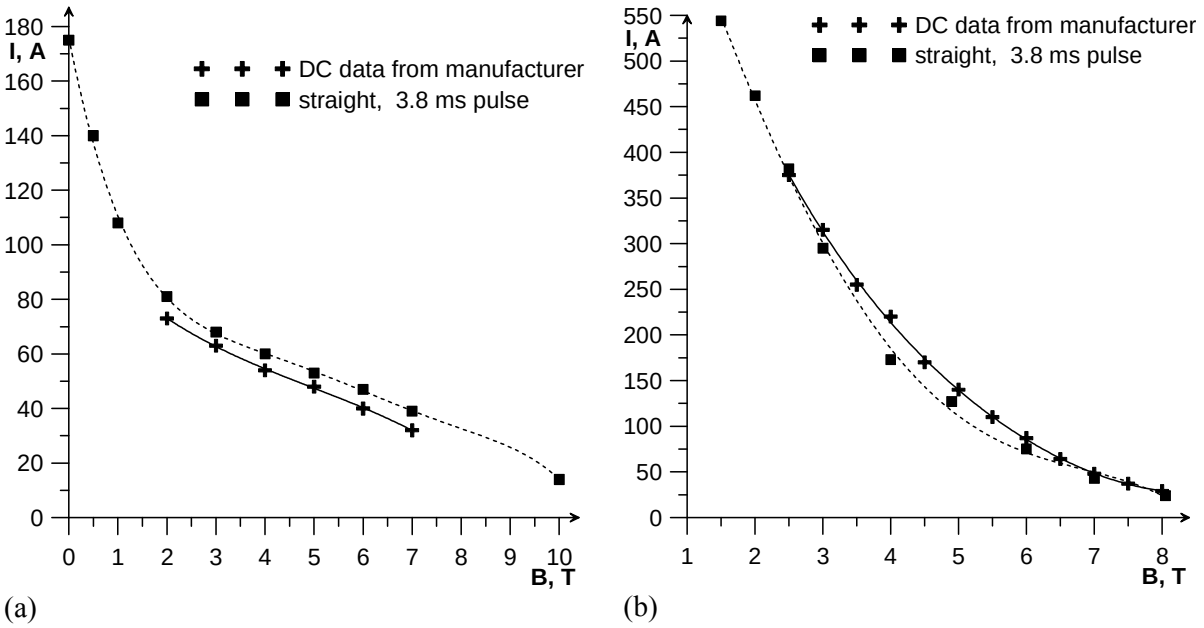

Figure 6. Transport critical current measurements (4.2 K) by DC and pulse techniques for: (a) the NbTi/Cu wire, (b) the MgB2/Ni/Fe/Cu tape.

However, large discrepancies – especially at low magnetic fields – were observed between DC and pulse measurements for a larger-diameter NbTi/CuMn/Cu wire (Luvata OK3900) with a more resistive CuMn interfilamentary matrix (figure 7) [6,7]. The critical current of NbTi/CuMn/Cu wire measured by pulsed techniques was very much lower than the DC value: the apparent critical current measured on a short straight sample was less than half of the DC critical current below 1T.

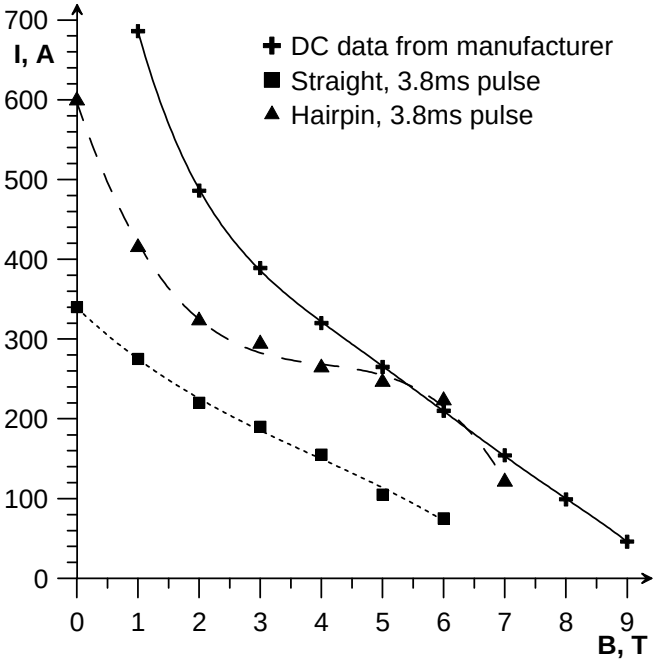

Figure 7. Critical current (4.2 K) data for NbTi/CuMn/Cu wire (OK3900) tested in DC conditions by the manufacturer, and in pulsed conditions using both short straight and hairpin samples.

Hairpin sample measurements of the NbTi/CuMn/Cu wire are in better agreement with DC measurements than those performed on a short straight sample, particularly at higher magnetic fields (figure 7). This might be explained by the differences in current contact size and spacing for the two

sample geometries. The current contacts were eight times longer for the U shaped (hairpin) sample than the straight sample, resulting in a lower contact resistance, and better matching the likely conditions for the manufacturer's DC critical current characterisation. However, whilst the straight sample geometry ensured that the testing current was always perpendicular to the external magnetic field, the hairpin sample had long lengths parallel to the applied field and significant curvature between the voltage taps. This changes the electromagnetic forces acting on the sample, the expected critical current (and hence, for a fixed current pulse duration, the rate of change of current), and the influence of self-field; all of which may contribute to the different shape of the Ic(B) curves for the two sample geometries [7]. In particular, the better agreement between DC measurements and pulse measurements on hairpin samples at high magnetic fields might be due to the lower self-field degradation of critical current or the lower rate of change of current. A detailed experimental study (beyond the scope of the present work), in which these variables can be controlled independently, is required to establish a complete explanation.

3.2. Modelling

The results of the analysis for the model with CuMn layers are presented in figures 8 and 9, which show current density and electric potential maps (respectively) along the wire at four different times during the modelled current pulse. Initially during the current pulse, the current flows mostly in the external NbTi cylinder (figure 8(a)) until the current density locally reaches the critical current density. Current flow through the external copper matrix and CuMn layer is driven by the potential difference between the current clamp and external NbTi cylinder (figure 9(a)). A flux flow resistivity appears in the external NbTi cylinder when its current density reaches J_c, allowing the electric field to appear in the external ring (figure 9(b)) and forcing excess current to the inner NbTi cylinder (figure 8(b)). The continuing increase in the applied current increases the current density in both NbTi cylinders (figure 8(b)), with some local instabilities as a result of highly resistive CuMn layers impeding current sharing between NbTi and Cu regions. The longitudinal potential gradient in figure 9(c) shows the length over which current is transferred from the copper matrix to the two NbTi cylinders through CuMn (figure 8(c)). Figures 8(d) and 9(d) show the situation after the transition to the normal state, when J_c has been exceeded in both NbTi regions. This voltage corresponds to the voltage measured on the wire after its transition to the normal state.

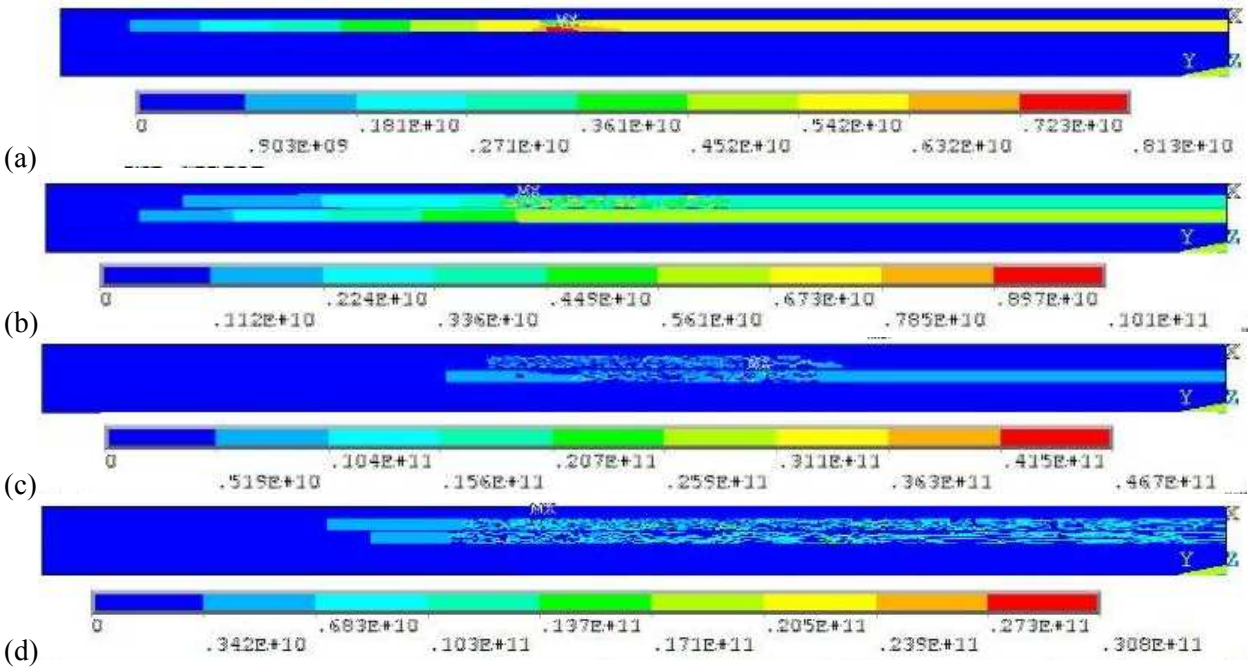

Figure 8. Current density along the wire for NbTi/CuMn/Cu wire: (a) t=0.8 ms, I=492 A, (b) t=1.06 ms, I=615 A, (c) t=1.32 ms, I=710 A, (d) t=1.605 ms, I=777 A.

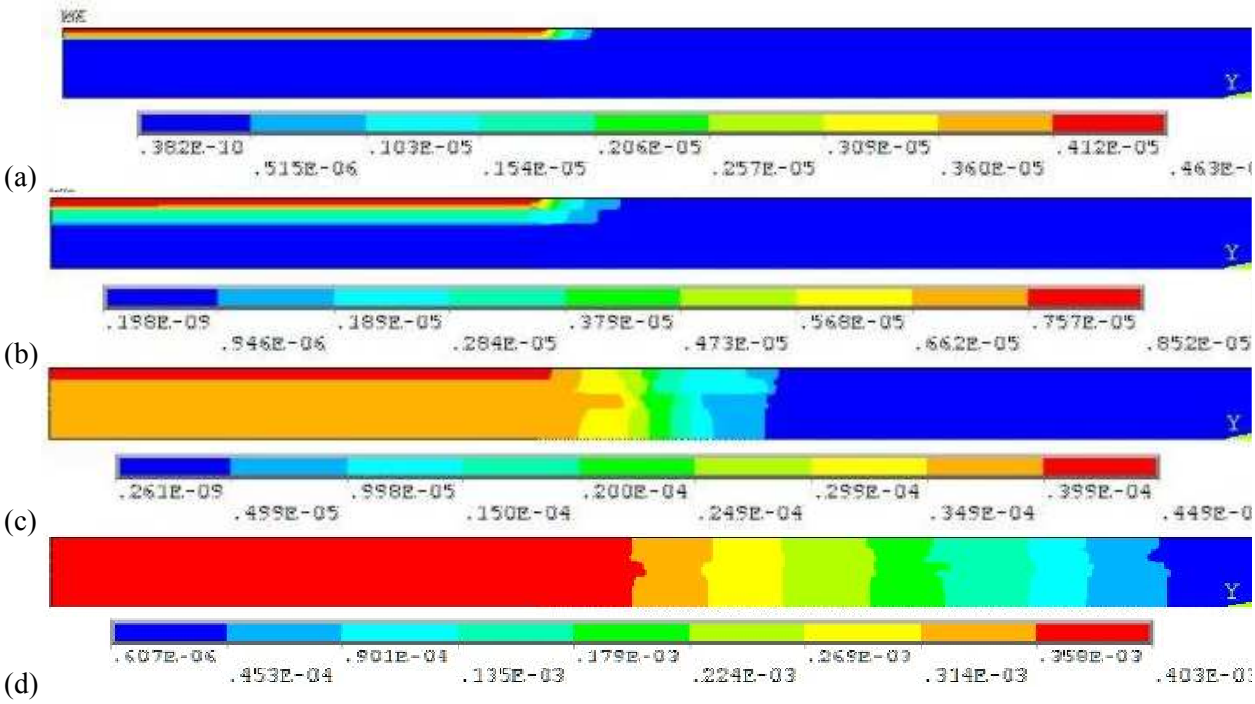

Figure 9. Electrical potential maps for NbTi/CuMn/Cu wire: (a) t=0.8 ms, I=492 A, (b) t=1.06 ms, I=615 A, (c) t=1.32 ms, I=710 A, (d) t=1.605 ms, I=777 A.

Figures 10 and 11 show the results when CuMn was replaced by copper, which is approximately 100 times less resistive. Early in the current pulse (I≈480 A), the current is much more evenly distributed between the NbTi cylinders with copper layers (figure 10(a)) than with CuMn (figure 8(a)). Current transfers into the inner NbTi cylinder over a much shorter distance for Cu (figure 10(b)) than CuMn (figure 8(b)) layers, and the current densities in the two NbTi regions approach equality within the short sample length studied here only for Cu layers (figure 10(b)).

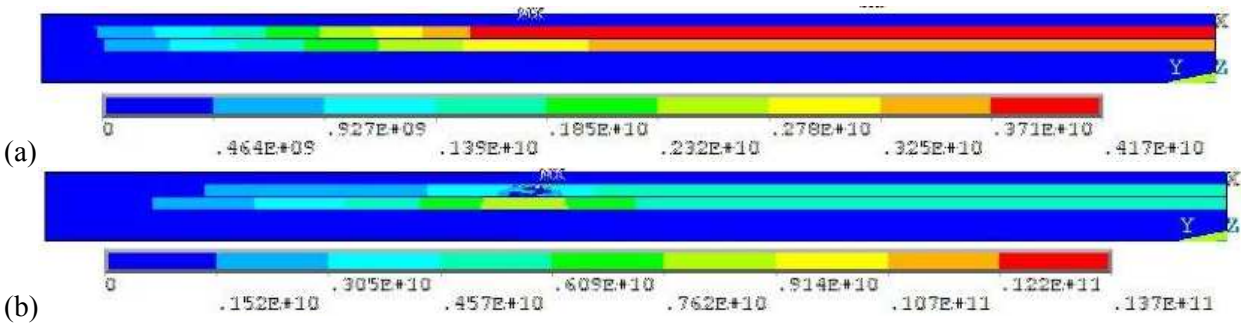

Figure 10. Current density along the wire for NbTi/Cu wire: (a) t=0.77 ms, I=476 A, (b) t=1.32 ms, I=710 A.

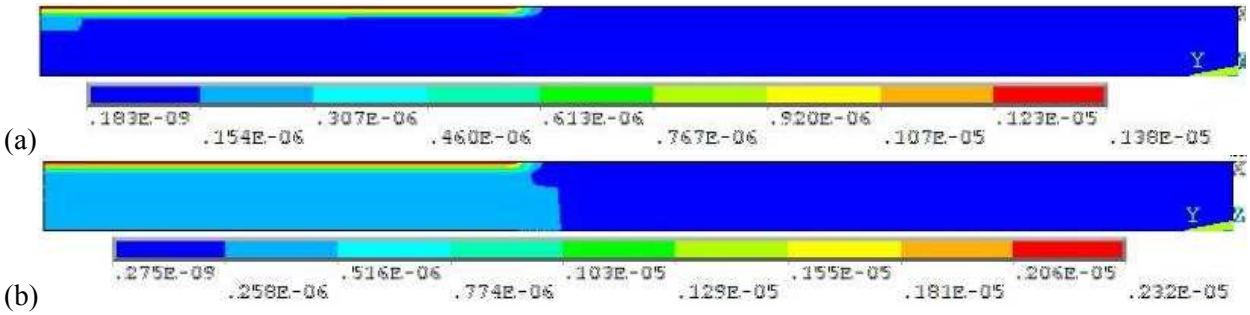

(a)

(b)

Figure 11. Electrical potential maps for NbTi/Cu wire: (a) t=0.77 ms, I=476 A, (b) t=1.32 ms, I=710 A.

These results clearly suggest that multifilamentary NbTi wires of the same architecture and critical current, differing only in interfilamentary matrix resistivity, may give different behaviour during pulse measurements. In particular, the current transfer length is longer, and the onset of a detectable voltage during a current pulse occurs at a lower current, for the wire with higher matrix resistivity. It should be noted that this does not take magnetic or thermal behaviour into account.

3.3. Discussion

As discussed above, the FEM modelling for a wire architecture closely resembling OK3900 suggest that differences in interfilamentary matrix resistivity are sufficient to significantly affect current sharing and the apparent critical current when measured using short samples in pulsed conditions. This is consistent with the experimental results for OK3900, for which the critical currents measured on short straight samples are very substantially suppressed below the manufacturer's DC values, but results for the longer hairpin samples are intermediate between the two (figure 7).

However, the MgB_2 tape investigated experimentally also has a high resistivity matrix (figure 3), but agreement between pulse measurements on short straight samples and the manufacturer's DC results is very good (figure 6(b)). Clearly matrix resistivity alone does not determine this behaviour. Several other factors are expected to be influential. There are differences in critical current criteria between DC and Cryo-BI-Pulse measurements, and differences in the sensitivity which can be achieved for different sample lengths and geometries. These seem unlikely to dominate here, as some of the conductors investigated here have similar critical currents and n values but differ greatly in the discrepancy between DC and pulsed results. Stability and AC losses might be significant factors, and the conductors discussed here differ greatly in these respects – indeed, the introduction of CuMn is designed to reduce losses – but the present model does not include the thermal and magnetic interactions required to analyse this behaviour. The introduction of these factors is a priority for future work.

Non-uniform distribution of current between filaments inevitably suppresses the critical current below that which would be achieved for equal current distribution, and this effect is expected to be more pronounced for wires with a larger number of layers of filaments [9]. This is consistent with the experimental observations reported here: OK3900, for which the largest discrepancy was observed, has the largest number of layers of filaments (21); and excellent agreement was found between pulse and DC measurements for both the NbTi wire A60/20 and the MgB_2 tape, which have only 4 and 1 layers respectively. The lack of current sharing difficulties with a single-layer construction may explain the consistent pulse and DC measurement results for MgB_2 despite its high matrix resistivity. Modelling is underway to investigate the effect of the number of concentric NbTi cylinders on the current distribution.

4. Conclusions

Excellent agreement has been found between DC and pulsed critical current measurements for a NbTi wire (A60/20) and a MgB_2 tape (Columbus Superconductors), but a large discrepancy exists between

DC and pulsed results for a different NbTi wire (OK3900). The NbTi wires differ mostly in interfilamentary matrix resistivity and the number, size and distribution of filaments (figure 3).

FEM modelling for pulse conditions has confirmed that increased interfilamentary matrix resistivity hinders current sharing and reduces the measured critical current. However, the model neglects thermal and magnetic contributions, and considers a simplified geometry with only two NbTi regions; and there is evidence to suggest that the number of layers of filaments and thermal considerations may contribute to the behaviour observed experimentally. Work is underway to introduce these factors to the model.

Acknowledgments
M. Woźniak gratefully acknowledges Siemens Magnet Technology for financial support.

References

[1] Goodrich L F, Fickett F R, *Cryogenics*, **22** (1982) 225–241
[2] Rogacki K, Gilewski A, Newson M, Jones H, Glowacki B A, Klamut J, *Supercond. Sci. Technol.* **15** (2002) 1151–1155
[3] Głowacki B A, Gilewski A, Rogacki K, Kursumovic A, Evetts J E, Jones H, Henson R, Tsukamoto O, *Physica C* **384** (2003) 205–210
[4] Stehr V, Tan K S, Hopkins S C, Glowacki B A, De Keyser A, Van Bockstal L, Deschagt J, *J. Phys.: Conf. Ser.* **43** (2006) 682–685
[5] Van Bockstal L, De Keyser A, Deschagt J, Hopkins S C, Glowacki B A, *Physica C* 839 (2007) 460–462
[6] Woźniak M, Hopkins S C, Glowacki B A, Janowski J, *Electrical Review*, **85** (2009) 198–199
[7] Woźniak M, Master's Thesis, Lublin University of Technology (2008)
[8] Wilson M N, *Cryogenics*, **48** (2008) 381–395
[9] Kajikawa K, Iiyama Y, Enpuku K, Funaki K, *Physica C*, **463–465** (2007) 852–856
[10] Ansys reference manual, Ansys Inc.